Available online at www.sciencedirect.com
SCIENCE DIRECT®

Journal of the European Ceramic Society 23 (2003) 2813–2819

www.elsevier.com/locate/jeurceramsoc

Study of the interfaces between austenite and ferrite grains in P/M duplex stainless steels

M. Campos[a,*], A. Bautista[a], D. Cáceres[b], J. Abenojar[a], J.M. Torralba[a]

[a]*Departamento de Ciencia de Materiales, Universidad Carlos III de Madrid, Adv. de la Universidad 30, E-28911 Leganés, Spain*
[b]*Departamento de Física, Universidad Carlos III de Madrid, Adv. de la Universidad 30, E-28911 Leganés, Spain*

Abstract

Duplex stainless steels produced by powder metallurgy (PM) can be obtained by two different methods. On one hand, a fully pre-alloyed powder with a duplex designed composition can be used as raw material; on the other hand, by mixing ferritic and austenitic powders into the desired proportion it is possible to achieve the required duplex microstructure. Through this second method, when austenite is <50 wt.%, materials show net duplex microstructures. But when the austenite percentage is higher than ferrite, a diffusion interface appears at grain boundaries, which modifies all the properties. The objective of this work is to characterize this interface in order to identify its nature and predict the behaviour of the duplex stainless steel. For this purpose, a duplex stainless steel has been produced by mixing ferritic–austenitic stainless steel grade powders, compacting at 700 MPa and sintering in vacuum at 1250 °C for 30 min. The mentioned interface has been studied by SEM and light optical microscopy (LOM) and characterized by nanoindentation in order to determine the hardness and Young's modulus of each phase. Testing mechanical properties completes the study.

Keywords: Duplex stainless steels; Nanoindentation; Powder metallurgy

1. Introduction

The duplex stainless steels (DSS) are an intermediate class between ferritic and austenitic stainless steels. Thus, these steels have the combined characteristic of both families. DSS are more resistant to stress corrosion but not quite as resistant as the ferritic ones; toughness is better than that of the ferritic steels but not as good as that of the austenitic. However, the strength of DSS is greater than that of austenitic ones. DSS were developed in the 1940s, but were not commercially produced until 1970s.[1]

Due to the optimum compromise between mechanical properties, corrosion resistance and economical advantages compared with austenitic stainless steels, DSS have increased their applications. The automotive industry is moving towards PM stainless steels for a wide range of applications, because by controlling the porosity it can achieve the requirements for exhaust systems, for example.[2]

Several authors have investigated the mechanical and corrosion behaviour of DSS obtained from mixed powders from ferritic, austenitic and even martensitic powder grades.[3–7] In the present work, the influence of the amount of ferrite–austenite on mechanical properties, due to the nickel and chromium diffusion, which promotes an interface on grain boundaries, has been investigated.

2. Experimental procedure

2.1. Involved raw materials

Water atomized 316L (austenitic) and 434 (ferritic) powders have been used as raw materials to prepare the different mixtures (Fig. 1). All of them were pressed at 700 MPa as tensile bars, and sintered at 1250 °C for 30 min with a cooling rate of 0.08 °C/s, in low vacuum ($P<10^{-2}$ atm) to prevent chromium losses.[8] Compositions and properties of powders are shown in Table 1.

2.2. Assessed properties

These samples have been used to measure the density, porosity features, microstructures, and mechanical properties following ASTM standards. The microstructural

* Corresponding author. Tel.: +34-91-624-9936; fax: +34-91-624-9430.
E-mail address: campos@ing.uc3m.es (M. Campos).

0955-2219/03/$ - see front matter © 2003 Elsevier Ltd. All rights reserved.
doi:10.1016/S0955-2219(03)00293-0

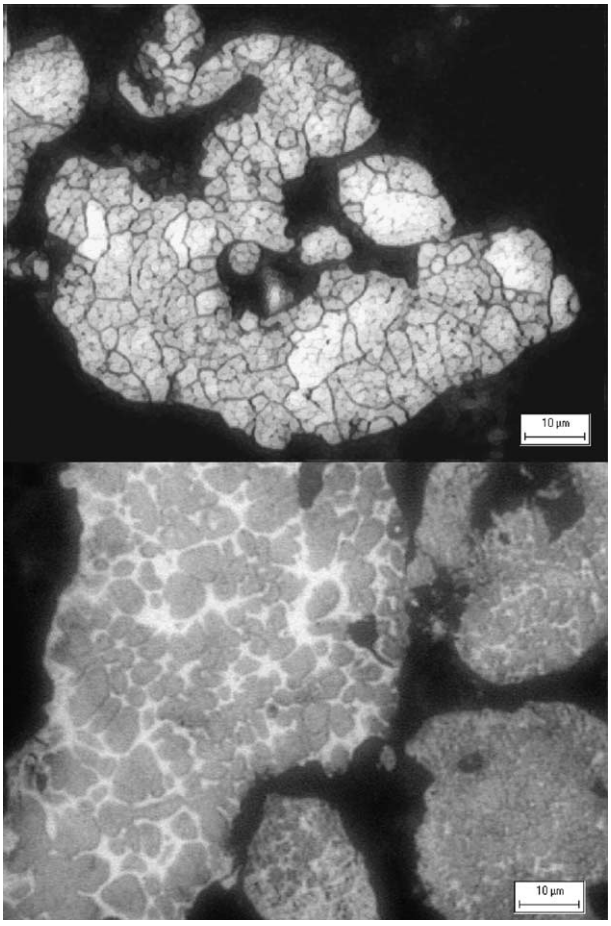

Fig. 1. Up: 434 powders. Down: 316L, the rapid cooling rate during atomized process promotes a-phase as matrix.

Table 1
Chemical composition of the base powders

Powder Grade	Composition				Flow (s/50 g)	Apparent density (g/cm^3)
	Cr	Ni	Mo	Si		
316L	16.40	13.2	2.50	0.90	27	2.93
434	16.73	–	1.09	0.80	26	2.89

study has been developed through light optical microscopy (LOM) and scanning electron microscopy (SEM); EDS has been used to evaluate the distribution of alloying elements on the different phases in the materials. Nanoindentation has been performed in order to characterize the inter-diffusion zone between ferrite and austenite grains. This test has been performed at room temperature with a Nanoindenter IIs (Nano Instrument, Inc, Knoxville, TN). Detailed nanoindentation experiments used in this characterization comprise of the following steps: approach indenter to sample surface at 10 nm/s; loading step until the total indenter displacement has reached 1000 nm; then, load is kept for 10 s to stabilize the measurement. The Oliver and Pharr method[9] has been followed to analyse the obtained load–displacement data, and hence hardness and elastic modulus are determined as a function of the indenter displacement.

The corrosion resistance of stainless steels and the potential microstructural complexity makes the best etchant selection a difficult problem. By adding glycerol as solvent a better wetting of the surface and a more uniform etching is provided. Methanolic aqua regia has been used to outline ferrite and reveal σ-phase if it is present. Beraha etchant (0.7 $K_2S_2O_5$ 20 ml HCl in 100 ml solution) has been used to develop duplex microstructures, as well as secondary phases.[10] Colour obtained after etching depends on composition, phase grain orientation, etching time and temperature.

3. Results and discussion

3.1. Microstructure features

Even though several authors had suggested Schaeffler's diagram to describe DSS microstructures,[6,11] due to the low cooling rate followed during sintering stage, it will be more convenient to considerer isothermal projected phase diagrams of ternary systems. These are more useful than even TTT diagrams for a DSS to determine secondary phases precipitation developed in Ref. 12, because no variation either of Cr or Mo is noticeable. Besides, in general, rapid cooling is necessary to prevent the precipitation of other phases.[13]

The self-diffusivity of iron into ferrite is approximately 100 times higher than in austenite, which promotes the higher densification level.[14,15] Due to this fact, to which sintering activity can be correlated, pores decrease as austenite decrease as well as sintered densities.[16,17] Higher pores are located at particle boundaries that coincide with interdiffusion area.

During the sintering process not only does iron diffusion take place, but also diffusion of nickel and chromium (see diagram of Fig. 2). The surrounding contact surface of austenitic and ferritic particles leads to diffusion of alloying elements and during the cooling stage leads to different phase transformations depending on composition.

The 75Ferrite–25Austenite DSS (Fig. 3) is first studied. In this case, the composition gradient is responsible for austenite transformation. During cooling from 1250 °C, the area surrounding particle boundaries follows the phase diagram proposed in Fig. 3 by Refs. 18 and 19. Some secondary austenite precipitates, leaving the core of the grain with the initial austenite phase. Some of the secondary austenite has an acicular or needle-like morphology, which can be seen clearly in Fig. 3. This kind of morphology can be achieved under slow cooling rates.[20,21]

When the percentage of austenitic powders is higher than ferrite, others phases can precipitate (shown in

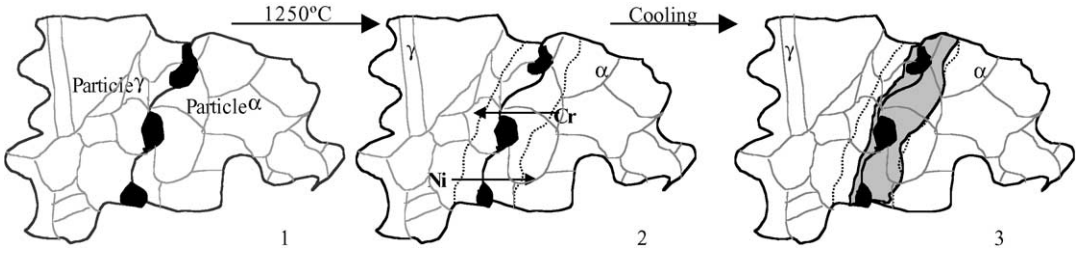

Fig. 2. Microstructural evolution during sintering process of mixed DSS.

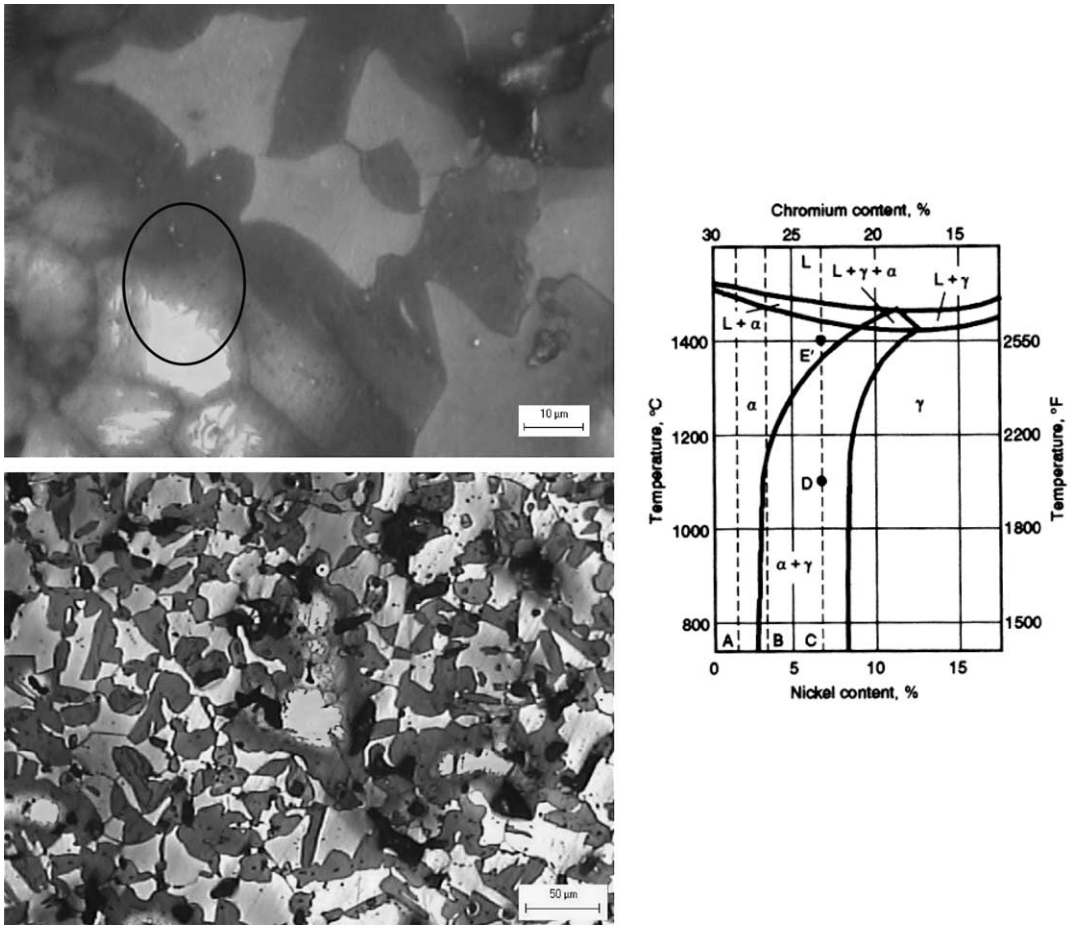

Fig. 3. Microstructure of 25Austenite–75Ferrite with Beraha etchant, upper in detail. Vertical section at 68 wt.%Fe of the Fe–Cr–Ni ternary system.[18]

Fig. 4). Some authors identify this constituent as a mixture of ferrite, austenite and martensite on the basis of Schaefller's diagram.[6] Although the phase morphology looks like a martensite phase, it has to be kept in mind that the carbon level is very low as well as an extremely slow cooling rate. Both facts must prevent the presence of martensite. Whenever austenite is in a higher proportion than ferrite, this interdiffusion zone always appears. Mixtures from 60Austenite–40Ferrite to 90Austenite–10Ferrite have been studied. The phase formation in the diffusion area might be caused by nickel diffusion from austenite to ferrite, by the energy excess on grain boundary, and the higher concentration of chromium in this area. This intermediate microstructure grows as subgrains, as can be seen in Fig. 5.

This intermediate phase, between ferritic and austenitic particles, has been also studied using SEM and EDS to show how there are differences in Ni and Cr concentrations. By line scanning it is detected that Cr decreases until austenite phase is reached, whereas Ni is present on ferrite grains. Hence, Ni and Cr composition shows a gradient from ferrite to austenite phases (see EDS results in Fig. 8). Following consecutive isothermal projections of Fe–Cr–Ni diagram,[22] this distribution of elements will lead to some σ-phase transformations but more importantly, to some mixture of α–γ that is very

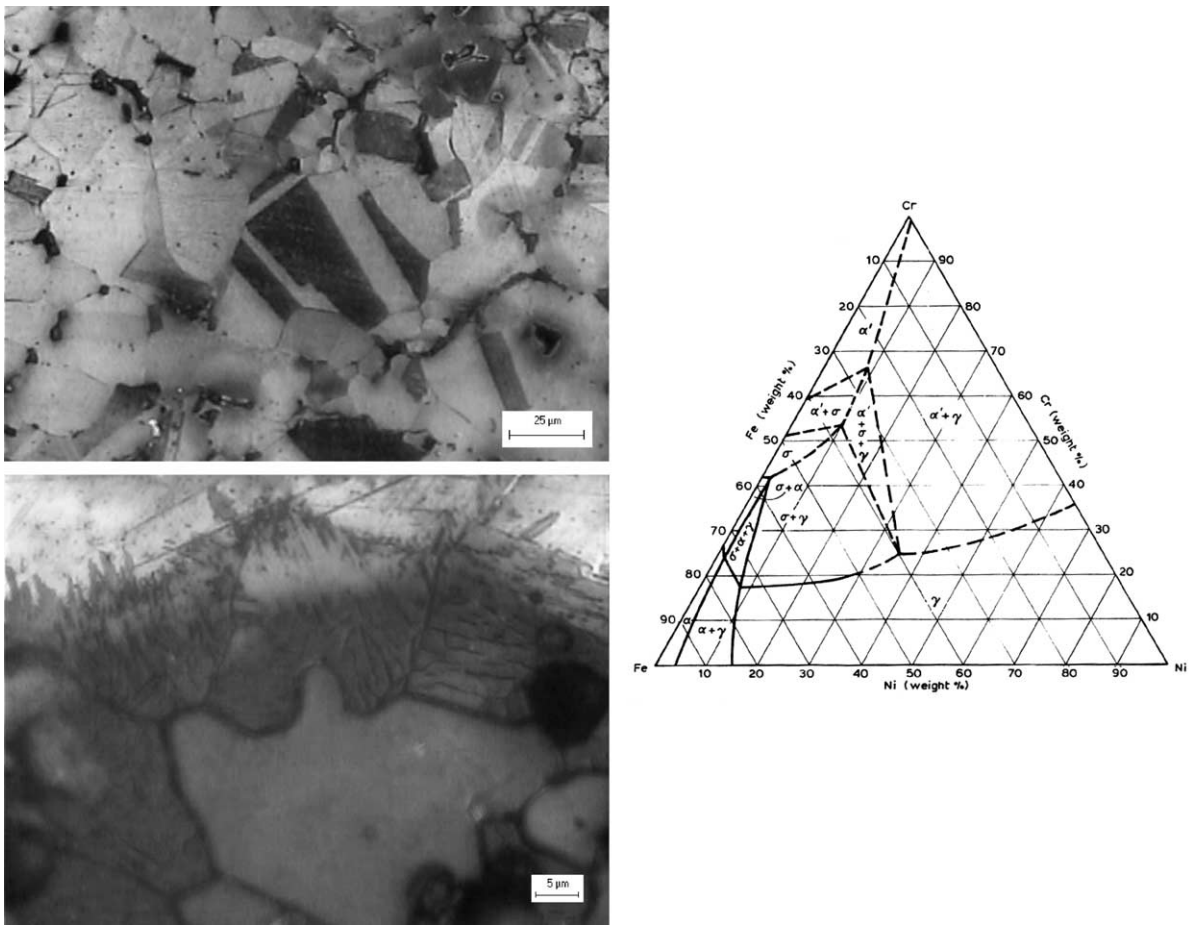

Fig. 4. DSS obtained from 85Aust–15Ferrite powder mixture. Up: austenite matrix. Down: inter-diffusion area between ferrite and austenite particles. Isothermal phase Fe–Ni–Cr diagram at 650 °C, showing the risk of σ-phase precipitation depending on local composition.[22]

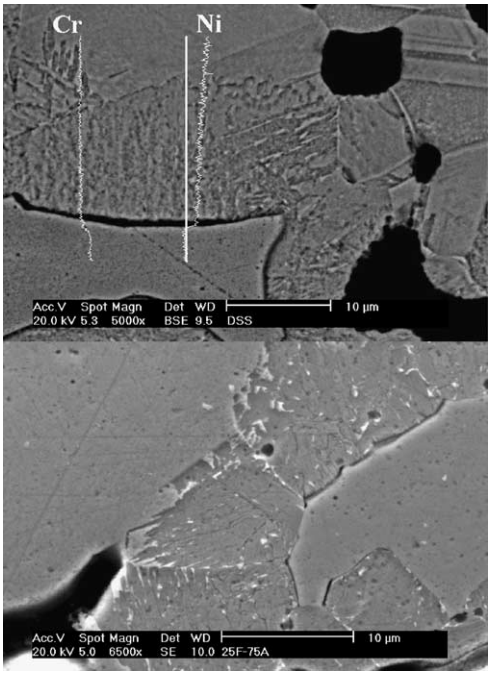

Fig. 5. Interface detail in DSS from 60Austenite–40Ferrite showing the Cr and Ni concentration, and 75A–25F detailing grain microstructure of precipitates.

thin and sharp and constitutes a DSS microstructure. Moreover, Mehara et al.[23] have shown how Ni contributes to accelerate σ-phase precipitation.

Microhardness follows Ni and Cr content and depends on DSS mixture, i.e. final composition and phase balance. Therefore, in the intermediate area of diffusion, microhardness has shown the biggest deviation (Fig. 6). Images of micro indentations measurements that show phases properties are presented in Fig. 7. Microhardness values are intermediate between ferrite and austenite, thus confirming its intermediate microstructure and the absence of martensite.

EDS results (Fig. 8) have revealed the composition evolution of the involved phases. Ni has enriched ferrite zones at the same time that austenite has lost it, and the inter-diffusion zone has reached a combination of element typically of DSS.

3.2. Nanoindentation

Nanohardness test provides mechanical properties of involved phases, as displayed in Table 2. This provides a better characterization of the inter diffusion zone. In monophase steels, values have shown a narrower

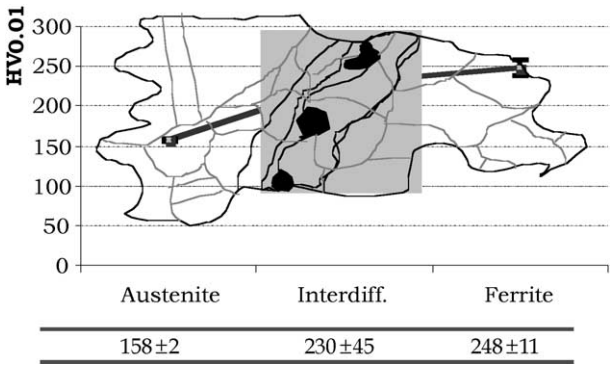

Fig. 6. Microhardness values on 85Austenite–15Ferrite DSS sintered mixture.

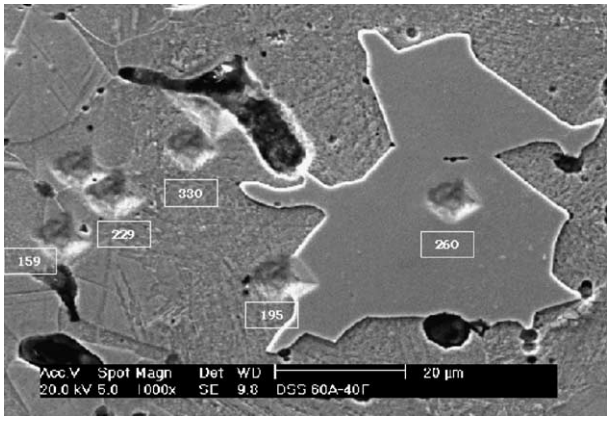

Fig. 7. Microhardness on 60Austenite–40Ferrite mixture.

deviation, whereas in mixed DSS the results strongly depend on compositions differences. The intermediate phase is closer to ferrite behaviour than to austenite, due to the high Cr and Ni content. By comparing both displayed DSS mixtures, it is shown how by decreasing Cr concentration (see EDS data) the hardness and

Table 2
Nanohardness depending on stainless steel class

100% Austenite					
H (GPa)	E(GPa)				
2.2±0.2	200±20				
100% Ferrite					
				H (GPa)	E(GPa)
				2.43±0.10	232±6
60Austenite–40Ferrite DSS					
Austenite		Intermediate Face		Ferrite	
H (GPa)	E(GPa)	H (GPa)	E(GPa)	H (GPa)	E(GPa)
2.6±0.3	182±14	3.8±0.2	187±13	3.8±0.2	204±7
80Austenite–20Ferrite DSS					
Austenite		Intermediate Face		Ferrite	
H (GPa)	E(GPa)	H (GPa)	E(GPa)	H (GPa)	E(GPa)
2.0±0.6	182±14	2.8±0.9	140±30	2.9±0.1	196±11

Young's modulus also decrease. Harder and tougher behaviour have been found in the middle of diffusion zone, where Cr and Ni offer the higher composition balance. In other words, when austenite is increased, hardness of inter diffusion area is decreased.

In order to show differences between phases behaviour due to elastic recovery, nanoindentations have been imaged by SEM (Fig. 9).

3.3. Mechanical properties

The hardness and strength level of the DSS processed from mixed powders, increases with increasing content of ferrite as in Ref. 24 due to enhancement of sintering mechanisms. The solid solution hardening of Ni and Mo of the ferrite phase, the internal strain hardening between ferrite and austenite due to different coefficient of thermal expansion, and the new inter-diffusion at particles boundary might be a few explanations for why

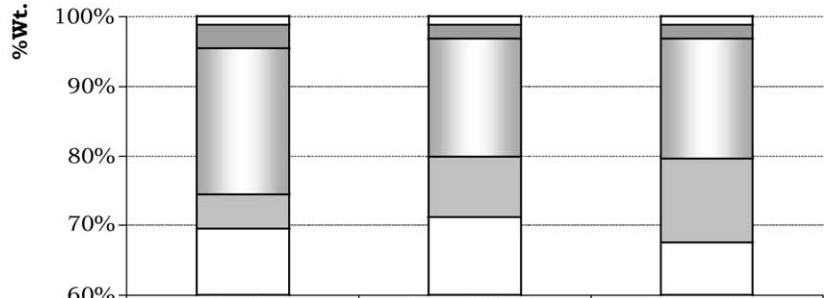

	Ferrite	Interdiffusion	Austenite
%Si	1	1	1
%Mo	4	2	2
%Cr	21	17	17
%Ni	5	9	12
%Fe	69	71	68

Fig. 8. EDS Analysis of 60 Austenite–40Ferrite DSS sintered mixtures. Precision of measured elements: Cr < 5%, Fe < 2%, Ni in ferrite < 8%, Ni in the rest < 3%. Because presence of Mo and Si is minority their precision is < 25%.

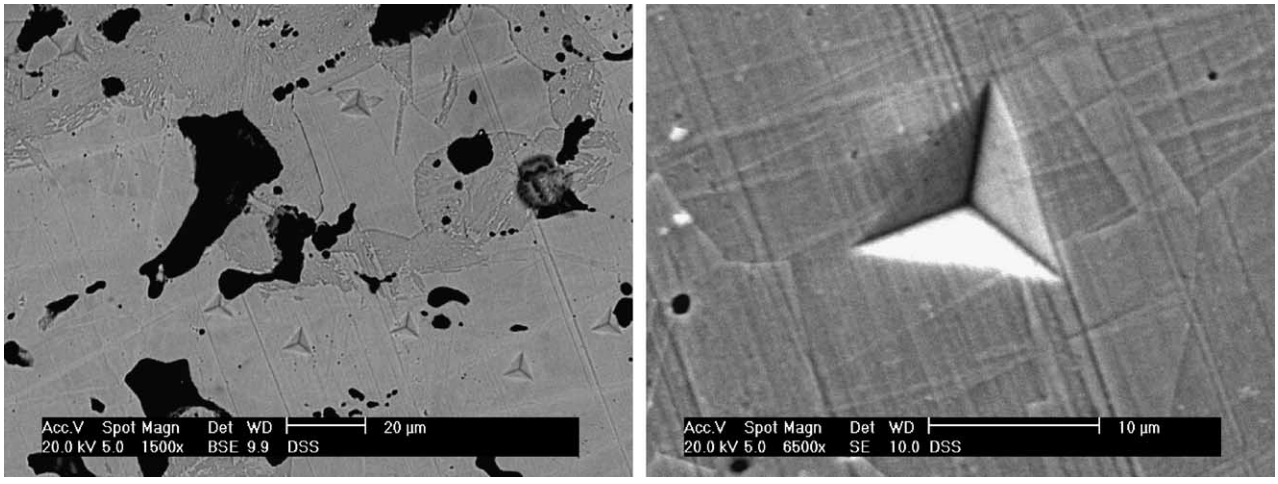

Fig. 9. Nanoindentation imaged by SEM.

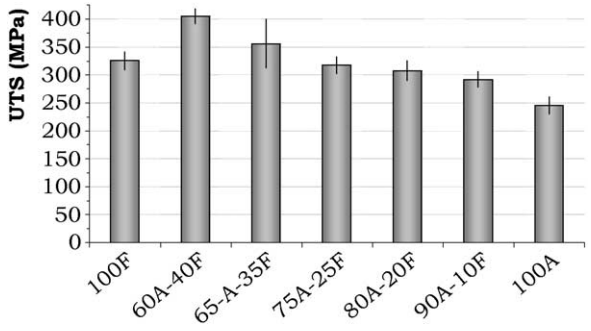

Fig. 10. Ultimate tensile stress depending on austenitic–ferritic powder balance.

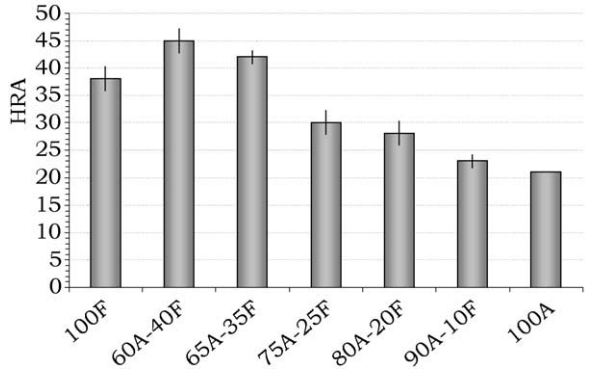

Fig. 11. Hardness depending on austenitic–ferritic powder balance.

the mechanical properties of DSS increase as compared with a monophase austenitic stainless steel (Figs. 10 and 11).

4. Conclusions

Duplex stainless steels obtained from ferritic and austenitic powders mixtures achieved a sintered microstructure that strongly depends on the balance of initial powders. Although a diphase-sintered microstructure is attainable, a real duplex microstructure is achieved during the cooling stage, surrounding the ferrite–austenite particle contacts where elemental diffusion leads to different Cr and Ni distributions.

When austenite is in lesser proportion than ferrite, secondary austenite precipitates on particle boundary. However, when austenite presence is the majority, a Ni concentration gradient develops from austenite to ferrite particle and leads to an interdiffusion zone that gives a local DSS with a sharp and thin microstructure.

The alloying system displays an enhancement of mechanical properties as a consequence of the solid solution hardening of Ni and Mo in the ferrite phase, the internal strain hardening between ferrite and austenite due to different coefficients of thermal expansion, and the new inter-diffusion area at particles boundary. All help to explain the mechanical properties improvement of DSS as compared with a monophase austenitic or ferritic stainless steel

Acknowledgements

The authors wish to thanks the financial support provided by the Spanish Ministry of Science and Technology through the project MAT2001-1123-CO3-01.

References

1. Charles, J., *The duplex stainless steels; Materials to meet your needs*. Beaune, France, 1991.
2. *Advanced Materials and Process*., 1998, **7**, 28–65.
3. Torralba, J. M., Moreira, W., Cambronero, L. E. G. and Ruíz Prieto, J. M., In *Proc. of 1993 Powder Metallurgy World Congress. Kyoto Japan*. pp. 517–520.
4. Torralba, J. M., Monsoriu, A., Ruíz-Román, J. M., Ibars, J. R. and Velasco, F., *Mater Proc, J. Tech*., 1995, **53**, 433–440.

5. Afify, N., Gaber, A., Mostafa, M. S. and Hussein, A. A., *Journal of Alloys and Compunds*, 1997, **259**, 135–139.
6. Marcu Puscas, T., Molinari, A., Kazior, J., Pieczonka, T. and Nykiel, M., *Powder Metall*., 2001, **44**, 48–52.
7. Marcu Puscas, T., Molinari, A., Kazior, J., Pieczonka, T. and Nykiel, M., In *Proc. of 2000 Powder Metall. World Congress*. pp. 980–983.
8. Paal, J., *Proc. of PM World Congress 1998, Special Interest Seminar*.
9. Oliver, W. C. and Pharr, G. M.. *J. Mater. Res*., 1992, 1564–1583.
10. *ASM Handbook, Vol. 9. Metallography and Microstructures*, 9th edn. 1992.
11. Rosso, M., Actis Grande, M. and Motoiu, P., In *Proc. of Euro PM 2000*. pp. 311–317.
12. Charles, J., In *Proc Duplex Stainless Steels Conf., Vol 1*. 1991. pp. 3–48.
13. Lula, R. A., *Stainless Steels*, 5th edn. American Society for Metals, NewYork, 1993.
14. Smithells, C. J., Brandes, E. A., ed., *Metals Reference Book, 5th edn*. Butterworths, London, 1976.
15. Hämäläinen et al., *Mater. Sci. and Tech*., February 1997, **13**.
16. Ruiz Prieto, J. M., Moreira, W., Torralba, J. M. and Cambronero, L. E. G., *Powder Metall*, 1994, **37**(1).
17. Campos, M., Sarasola, P., Torralba, J. M., In *Proc of 9th International Scientific Conference: "Achievements in Mechanical & Materials Engineering"*. 2002, pp. 83–86.
18. Birgham, R. J. and Tozer, E. W., *Corr*., 1974, **30**(5), 161–166.
19. Colombier, L., Hochmannn, J.. Edward Arnold Ltd, Stainless and Heat resisting steels, 1967.
20. and Ceylan, M. *et al*., *Journal of Materials Processing Technology*, 1997, **69**, 238–246.
21. Solomon, H. D., Age Hardneing in a duplex staniless steel. In *Duplex Stainless Steels*, ed. R. A. Lula. America Society for Metals, 1983, pp. 12–15.
22. West, D. R. F., *Ternary Equilibrium Diagrams. 2nd edn*. Chapman & Hall, 1992.
23. Mehara, Y. et al., *Met. Sci*., 1983, **17**, 541.
24. *Powder Metall*., 1994, **37**(1), 57–60.